IV Conferencia Panamericana de END
Buenos Aires – Octubre 2007

AAENDE
Asociación Argentina de Ensayos No Destructivos y Estructurales

Phase unwrapping applied to portable digital shearography

Dirk Findeis, Jasson Gryzagoridis, Emlind Asur
Department of Mechanical Engineering
University of Cape Town, Private Bag, Rondebosch, 7700
Tel: +27 21 6503670
Fax +27 21 6503240
Dirk.findeis@uct.ac.za

Abstract

Digital Shearography is an Optical non-destructive testing technique, suitable for the inspection of manufactured components for defects. The technique employs the correlation of speckle images before and after object deformation and is particularly suited for inspecting composites for a range of defects including internal debonds and delaminations. The Department of Mechanical Engineering at the University of Cape Town has developed a portable Digital Shearography system which has the ability to perform phase stepped inspections. In addition, a software project has just been completed which complements the existing software by unwrapping the phase fringes into a displacement gradient map.

This paper describes the principle of Digital Shearography, before highlighting the development of the portable Digital Shearography system. Selected aircraft composite samples from a carbon fibre helicopter rotor blade are then subjected to phase stepped shearography inspections using the new system. The developed phase unwrapping algorithm is described and then applied to the obtained fringe patterns and the results presented. The paper is concluded with an evaluation and discussion of the complete system.

1. Introduction

If one has a closer look at the industries associated with the development and manufacture of automotive, aerospace, weapons, defence and boating products, the increased use of composite materials is an apparent trend. This is mainly because of their excellent strength to weight ratios, structural rigidity and strangely enough also structural flexibility depending upon the design, as well as their inertness to the weakening effects of corrosion. Some of the visible benefits to us include improved performance when using for example carbon fibre tennis or squash rackets or composite racing bicycles. Other benefits include a more comfortable cabin pressure when flying in the new Airbus A380 or Boeing Dreamliner aircrafts. The benefits to the manufacturer include lighter yet stronger finished products resulting in improved overall performance, reduced machining costs due to the mouldable nature and thus better integration of the composite materials, potentially longer life expectancy of the finished

item, as well as reduced energy consumptions for the aerospace industry, to name but a few.

Irrespective of what material was used, the finished product might include minor defects due to the manufacturing process and will most certainly acquire and accumulate defects over time. This weakens the component which is where the challenge to the industry lies; to monitor the progressive degradation of the component and remove it from service before a potentially catastrophic and costly failure occurs. To determine the integrity and serviceability of composite structures or components, non-destructive methods of testing are required both during manufacture as well as during their service or operation. An alternative approach is to replace components at predetermined intervals, as specified by the manufacturer, without applying any routine NDT inspection techniques at all. This however is obviously not feasible for items such as aircraft fuselages, ship hulls, yacht masts and helicopter blades, to name but a few.

When it comes to suitable NDT inspection techniques, engineering NDE professionals will agree that no single technique provides the total solution to all material and defect types and that it is best that a combination of NDT techniques be employed. We at the University of Cape Town, and others, have determined that ESPI and Digital Shearography are particularly well suited for defect detection in composite materials[1,2,3,4]. As a result, researchers in the Department of Mechanical Engineering embarked on a project to develop portable NDT equipment based on the principles of Electronic Speckle Pattern Interferometry ESPI and Digital Shearography[1,2,4]. This paper discusses the advances made on the portable DS prototype.

2. Theory

Digital Shearography is a non-contacting, whole field optical interference technique[4] which has the ability to reveal the presence of flaws or defects as localized disturbances in a generated fringe pattern[1,2,3,4,5]. These fringe patterns depict the gradient of surface displacements on the test object in response to an applied stress such as mechanical, thermal, pressure or vacuum stressing. Fringe anomalies reveal the position and approximate size of the defect, but not its depth relative to the surface. A typical

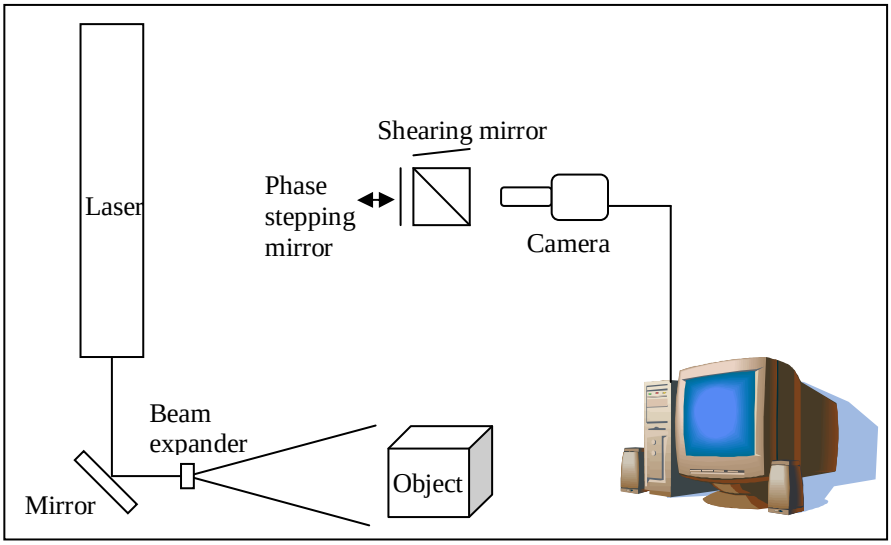

Figure 1. Typical Shearography set-up

Shearographic setup is depicted in figure 1 above. A single wavelength laser light source is expanded and used to illuminate the object. The speckular reflection off the object is viewed with a camera, through a shearing device. A modified Michelson interferometer, a glass wedge or a bi-refringent prism are commonly utilized to shear the image. The Michelson interferometer type is preferred by the authors in that it allows for greater flexibility to vary the magnitude of the shear, which controls the sensitivity of the system.

The function of the shearing device is twofold, the first being to take the incoming speckle image and split it into two separate images. By introducing a tilt on one of the mirrors, the reflected images, when recombined by the beamsplitter cube, are sheared into two distinct overlapping images and can be controlled by the amount of mirror tilt. The second function of the shearing device is to introduce discrete phase shifts of one of the sheared images by changing the path length of one of the sheared images. For this purpose the second mirror is attached to an externally controlled linear micro stepper.

Because a monochromatic light source is used, the shearing process is a collection of the interference of two neighbouring points on the object combined into one, which forms a speckle pattern and is captured and stored as the reference image in a PC. The next step is to stress the object to cause its surface to deform. The two adjacent points referred to above will change positions and hence their optical path lengths will change. This produces a new speckle interference pattern, which is also captured. By subtracting the two stored images from one another, the difference in intensity of the two images can be represented as[6] :

$$I_{\Delta} = 2I_0 \left[\sin\left(\alpha + \frac{\delta}{2} \right) \right] \sin\frac{\delta}{2} \qquad (1)$$

where: I_0 = intensity of the laterally sheared images,

α = phase difference between the two neighbouring points on the surface of the first stored image, and

δ = relative phase change of the two neighbouring pixels after the stressing process.

The visual result of the above is an image with black and white fringes, where each additional fringe represents a change in the displacement gradient magnitude *δp/δx (or y)*. This gradient magnitude can be obtained via equation 2 below:

$$\frac{\delta p}{\delta x} = \frac{\lambda N}{2S} \qquad (2)$$

where: λ = wave length of the laser,

N = number of fringes observed, and

S = variable lateral shear imposed.

The above process produces intensity based fringe patterns, which do not provide any information regarding the direction of the object displacement rate. In order to quantify this, the phase of the laser can be modulated using a technique called phase stepping. Using the micro phase stepper, 4 instead of only 1 images are captured both before and after the image is stressed. Between each image acquisition the stepper mirror is adjusted by an amount equal to an increase of (λ/4) of the beam path length, which

corresponds to a phase change of (π/2) in the image. The intensities of the 4 images can be represented in equation 3 as follows[7]:

$$I_i(x,y) = I_B(x,y) + I_{MP}(x,y)\cos(\theta(x,y) + i \cdot \pi/2) \quad (3)$$

$$\phi(x,y) = \arctan\left(\frac{I_3(x,y) - I_1(x,y)}{I_4(x,y) - I_2(x,y)}\right) \quad (4)$$

$$\beta(x,y) = \phi_a(x,y) - \phi_b(x,y) \quad (5)$$

where i = 1,2,3,4
I_B = intensity of the background noise
I_{MP} = intensity of the modulated phase
θ = phase of the 2 interfering neighbouring pixels
$\phi_a(x,y)$ = phase distribution after stressing,
$\phi_b(x,y)$ = phase distribution before stressing

Equation 4 determines the phase distribution of the speckle interference pattern and eliminates the background noise, represented by $I_B(x,y)$. By determining the phase distribution both before and after the object is stressed, equation 5 can be used to calculate the change in phase of the laser light due to the object surface displacement. As β repeats itself at 2π intervals, the fringes in the resultant image are of a saw tooth profile and the slope of the profile is used to determine the direction of object movement. Equation 2 can be used to determine the magnitude of the displacement gradient.

3. Digital shearography prototype

All of the above was encapsulated into a portable Digital Shearography prototype[4] as seen in figure 2 below. The unit is self contained and includes the camera, diode laser, shearing optics and phase stepper. The system is controlled by a PC and custom written

Figure 2. Portable Digital Shearography prototype

software which sets up and adjusts the camera and framegrabber controls, performs the various image acquisition procedures, phase stepping sequences, and image processing routines including variable sine and cosine filtering routines. An NDT inspection sequence is performed in real- time, meaning that the displayed intensity or phased stepped fringe patterns in response to the applied stress are updated in real-time.

The filtered phase stepping fringe patterns readily reveal the presence of a defect as shown on the PC monitor in figure 3. The direction of the displacement gradient can also be seen via the direction of the greyscale gradient. To make the evaluation as user friendly as possible these phase maps need to be unwrapped into a single displacement map, where each greyscale represents a unique displacement gradient level, which was part of the recent developments for the portable system.

3.1. Phase Unwrapping

In order to unwrap the images, the software process was broken down into a number of steps. In the first step the entire image is scanned in order to locate the fringe discontinuities. This can be done by monitoring the grey scale level of a pixel in relation to its surrounding pixels. Where an abrupt change in intensity occurs, the cause is one of two things, either the edge of a fringe is encountered or image noise is encountered. A threshold value is used to determine whether the intensity discontinuity is a fringe or noise. From this process, an image mask is created which is essentially a black image with white lines locating the identified phase fringe edges.

The next step in the sequence is to discretise the phase image into a set of blocks. Each block is then processed sequentially. By using the image mask to determine whether the block contains a section of a fringe or not, one of two processes occur. If no fringe is present, it is first determined whether the gradient is positive or negative and the sign of the greyscale value adjusted accordingly. The values of the last column of the previous block are then simply added to all grey scale values of the current block and written into a new image buffer. Where a block does contain a fringe, the sign of the fringe gradient is first determined before the sign of the greyscale values in the block is set. Once completed, the values of this block are added to and stored in the image buffer as described above. This process continues until the whole phase stepped image has been processed.

The image buffer now contains data which is an accumulation of the phase fringes. The maximum and minimum values are determined and the entire image rescaled to values ranging from 0 to 255 in order to display the unwrapped image as a greyscale. Using equation 2 and with prior knowledge of the magnitude of shear and wavelength of the laser light, the image buffer can also be rescaled to represent the magnitude of the displacement gradient.

By scanning through the scaled displacement gradient image, and adding the magnitude of the displacement gradients pixel by pixel to the previous pixel and storing the accumulated result in a new image buffer, the object displacement as a result of the applied stress can be reconstructed into a displacement map.

The imaging routines described above can then either be displayed as 2D grey scale images or with the help of MatLab as 3D surface maps.

4. Results

After completion, the new software was loaded onto the portable system and tested on a 300mm section of an Oryx helicopter rotor blade. The composite structure of the blade was made up of a carbon fiber outer skin with plywood inserts, fibreglass, carbon fiber and resin for the spar, honeycomb for the core of the blade, and a curved stainless steel plate around the leading edge for protection. Three defects were created in the sample section by cutting three 48mm diameter holes of varying depth into the rear side of the surface. This meant that the defects where invisible when viewed from the inspection side of the blade, as seen in figure 3 below. An infra red lamp connected to a dimmer

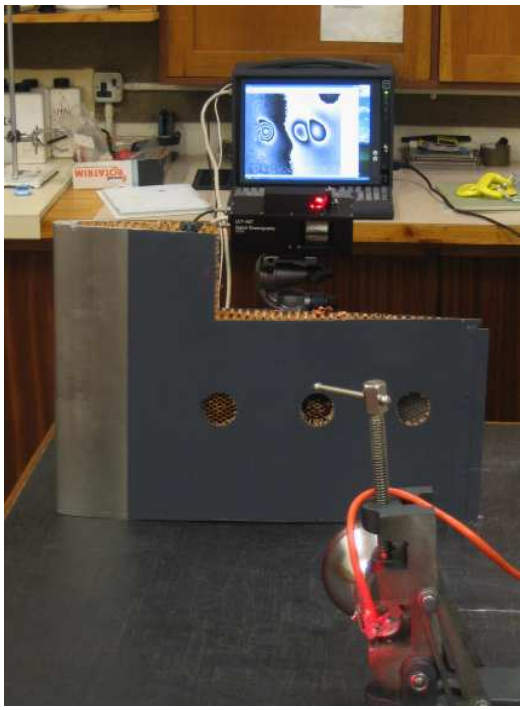

Figure 3. Helicopter blade section With man-made defects

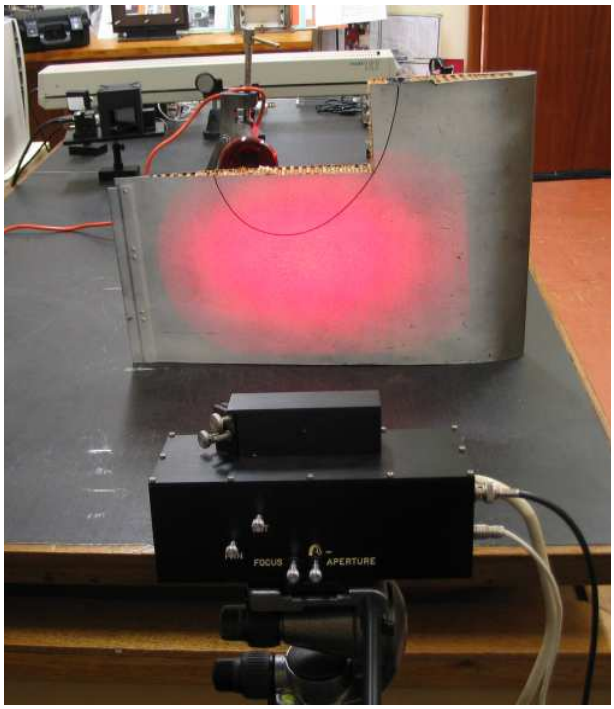

Figure 4. Front view of illuminated sample

and timer was placed behind the blade, and switched on for 5 seconds at a time in order to stress the object during the inspection process. The Shearography head and industrial PC can be seen in the background in figure 3 and the front view of the laser illuminated sample as well as the rear of the Shearography head unit can be seen in figure 4 above.

The following images are the results of the inspection process. In the first set of images, the central flaw was investigated. This flaw had its rear skin and part of the honeycomb core removed. For this inspection set, the phase stepping sequence was initiated, and once in real-time mode the heat was applied for 5 seconds. Approximated 10 seconds later, the continuous phase stepping sequence was halted and the final image filtered. The result can be seen in figure 5 below which clearly reveal the double bulls-eye fringe pattern, indicating the location of the sub-surface defect. This image was then subjected

to the phase unwrapping routine, which is called up by clicking a push button on the floating toolbar. The image generated by this post processing routine is revealed in figure 6 alongside and took approximately 0.5s to generate. The accumulation of the positive displacement gradients on the left of the image produce the elliptical white section on the left and the accumulation of the negative gradients on the right of figure 5 result in the elliptical dark section in the unwrapped image. The location of the defect

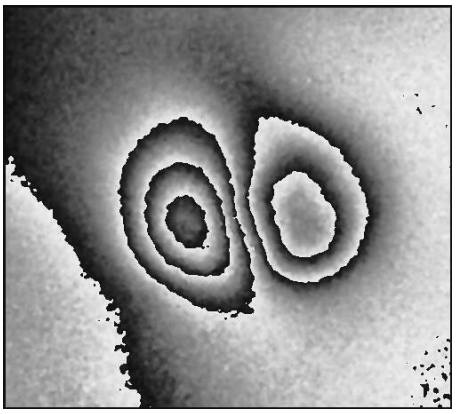

Figure 5. Phase map of single defect.

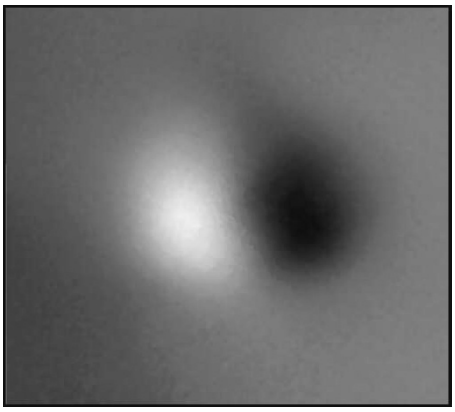

Figure 6. Phase unwrapped image of single defect.

can clearly be identified and stands out from the rest of the image in figure 6. This image was manipulated using the Matlab "mesh" function in order to produce a 3D map of the intensity of the unwrapped image. The result is presented in figure 7 below. Here

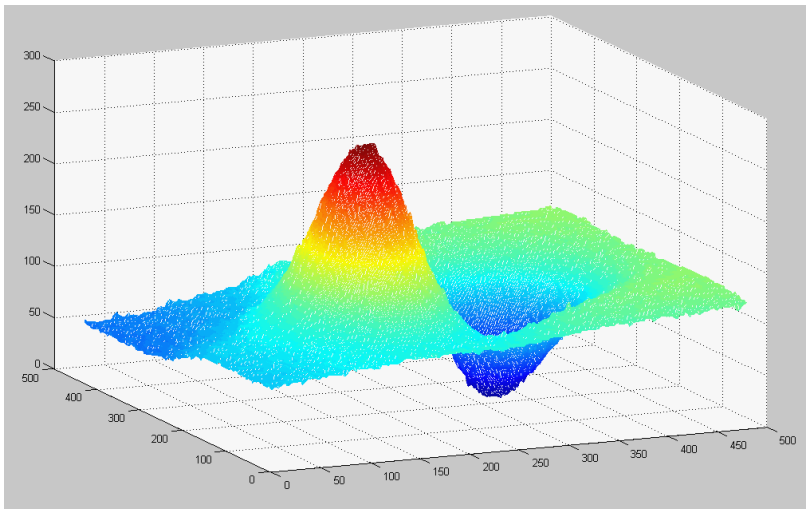

Figure 7. Matlab 3D visualisation of the unwrapped phase image

one can clearly see the change in displacement gradient magnitudes, both positive and negative, across the image. This form of representation also clearly reveals the difference in gradient magnitudes between the flawed section and the defect free area.

The greyscale image was subjected to the reconstruction routine by clicking another push button on the floating toolbar. The result of this image processing routine can be seen in figure 8 below. Here the presence and location of the defect can clearly been

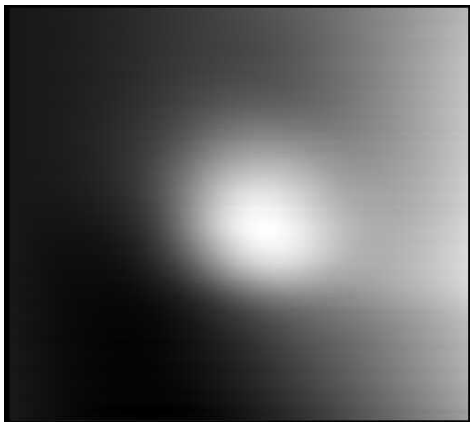

Figure 8. Reconstructed displacement image.

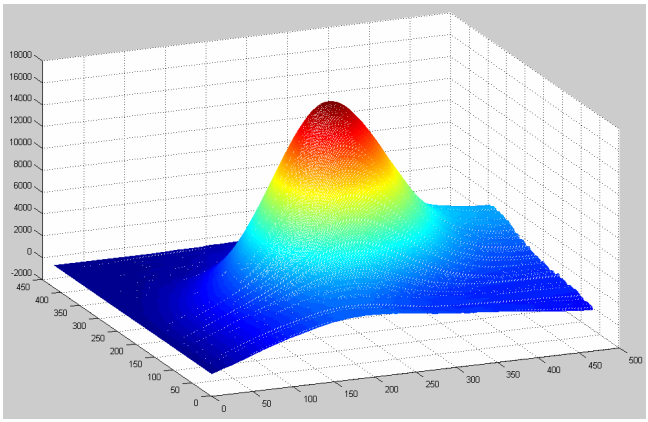

Figure 9. Matlab 3D visualisation of reconstructed image.

seen as the white circular section indication a larger displacement than the immediate surrounding due to the weakened structure. This image was also subjected to the Matlab "mesh" function and is illustrated in figure 9 alongside. Here the presence of the defect is identified by the conical section in the centre of the image protruding from rest of the surface.

The helicopter blade section was then re-positioned so that two defects could be seen simultaneously. Because the man-made defect positions relative to the thickness of the blade, as well as the depth were all different, the aim of this test was to see whether a difference in defect severity could be noted in the results.

Figure 10 below shows the phase map of the two defects viewed during the inspection process. The presence and location can clearly be determined through the presence of

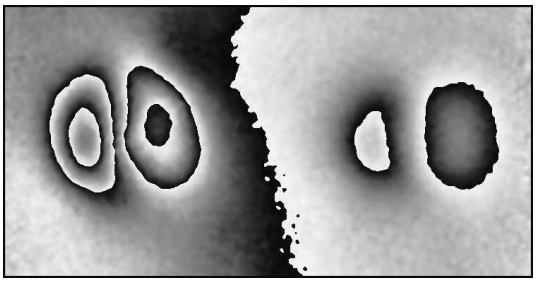

Figure 10. Phase map of 2 defects

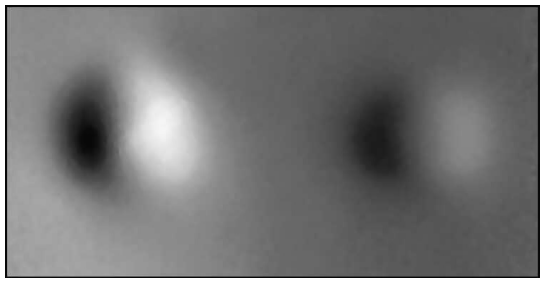

Figure 11. Unwrapped phase map of 2 defects.

two sets of bulls-eyes, the left set revealing a higher fringe density than the right set. Figure 11 is the unwrapped result of figure 10. Here too the different fringe densities of the two defects can be seen in the greater contrast between the bright and dark sections of the left hand fringe, when compared with the right hand fringe. Figure 11 was then subjected to the same Matlab treatment and is shown in figure 12. Here the 3D surface

reveals not only the position and direction of the displacement gradients produced due to the defects, but also the relative difference in magnitude of the two sets of gradients.

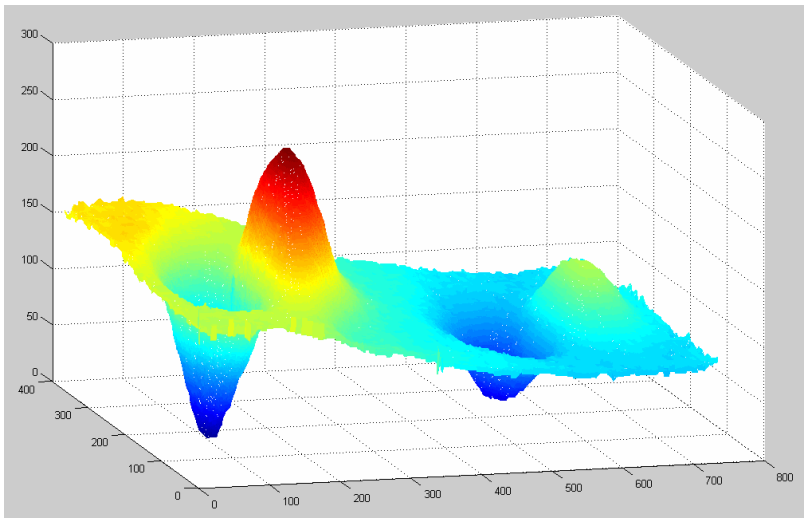

Figure 12. 3D Matlab rendering of the unwrapped phase image.

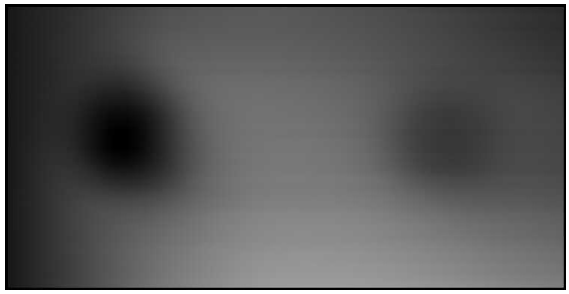

Figure 13. Reconstructed displacement image of defects.

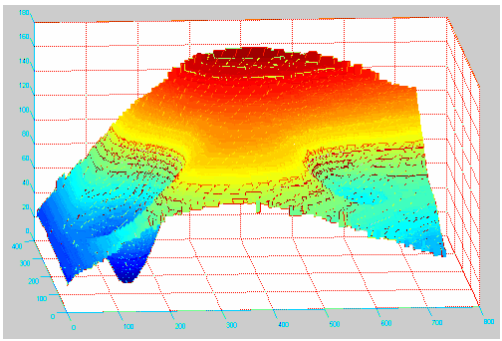

Figure 14. 3D Matlab surface map of displacement image.

The reconstructed displacement image is depicted in figure 13 and the 3D Matlab surface map in figure 14. This representation clearly identifies the defects and the difference in greyscales between the two defects hints at the greater severity of the left defect over the right defect. The Matlab 3D map also reveals the shape of the overall surface deformation in response to the applied heat and in addition indicates that the centre of the heat lamp was located centrally between, but below the two defects. This is evidenced by the red region in the figure 14 pointing to where the greatest displacement during the test occurred.

What also should be noted is that the sequence of bright and dark displacement gradients in figure 11 has been reversed when compared with figure 6. This is because for the second inspection procedure the image was first heated before the reference set of images were captured. The image was then allowed to cool down, i.e. the object was allowed to relax back to its original position, which is the reverse of the first test sequence. The displacement gradients should therefore be reversed, which is confirmed by the results in figures 10 through 14.

5. Conclusions and recommendations

The above results show that the phase unwrapping routines recently developed and implemented into the portable Digital Shearography prototype software are functioning and produce valid grey scale images, which conclusively reveal the presence of defects. The images appear to be unambiguous in terms of locating the fringes, in that the repetitive saw tooth fringes are removed from the images. The results also capture the direction of object movement in response to the applied stress, indicating that the code correctly identified the sign of the displacement gradient direction. The code also correctly assigns the grey scale range to the accumulated data. This is observed with the two defect sets of results, where the severity of the displacement gradient and reconstructed displacements is distinguishable in the grey scale of the images. The 3D maps add a further dimension to the visualisation of the defects present.

The added code simplifies the identification of defects present in inspected components. A benefit would be to assign magnitude levels to the grey scale levels in order to fully quantify the defect magnitude. This would have to include a means of entering the magnification factor and shear magnitude for each test in order to obtain valid test results.

Horizontal lines can be seen in some of the presented results. This is because the process occurred from left to right and background noise which was still present in the marginally filtered phase maps is accumulated as the procedure progresses through the image. It could be considered to devise a combined horizontal and vertical phase unwrapping sequence to reduce this effect.

The time required for the above post processing routines was in the order of 0.5 seconds for each image which was only achieved by using a masking interface to select the area of interest in the whole image. The processing time does increase if the whole image is processed; the time required depending on how much noise is present beyond the boundaries of the image.

The 3D visualisations are useful and should be considered for inclusion into the software package.

6. References

1. D Findeis, J Gryzagoridis, “A Comparison of the Capabilities of Portable Shearography and Portable Electronic Speckle Pattern Interferometry”, Proceedings of Nondestructive Evaluation and Health Monitoring of Aerospace Materials and Civil Infrastructure, P J Skull, v5393, pp41-49, 2004.

2. J Gryzagoridis and D Findeis “Simultaneous Shearographic and Thermographic NDT of Aerospace Materials”, Insight 48/5, p 294-297, 2006.

3. Erne, T Waltz and A Ettemeyer “Composite Structural Integrity NDT with Automatic Shearography Measurements”, ASNT publications, Dec 2000.

4. D Findeis, J Gryzagoridis, M Matlali, “Phase Stepping Shearography and Electronic Speckle Pattern Interferometry”, Proceedings of Third US-Japan Symposium on Advancing Applications and Capabilities in NDE, CD-Rom, ISBN 1-57117-133-9, 2005.

5. R Jones, C Wykes, Holographic and Speckle Interferometry, 2nd Ed. Cambridge University Press, 1989.

6. Y Y Hung , “A speckle-shearing interferometer: a tool for measuring derivatives of surface displacement”, Opt. Commun. 11 (2), pp132-135, 1974.

7. AM Maas, PM Somers, “Two-dimensional Deconvolution Applied to Phase-stepped shearography”, Optics and Lasers Engineering, 26, pp351-360, 1997.